J Mater Sci (2012) 47:6768–6776
DOI 10.1007/s10853-012-6592-y

Hydrogen depth profile in phosphorus-doped, oxygen-free copper after cathodic charging

Åsa Martinsson · Rolf Sandström

Received: 17 February 2012 / Accepted: 17 May 2012 / Published online: 29 June 2012

Abstract Spent nuclear fuel, in Sweden, is planned to be put in 50-mm thick copper canisters and placed in 500-m depth in the bedrock. Depending on the conditions in the repository, an uptake of hydrogen in the copper may occur. It is therefore necessary to establish how a hydrogen uptake affects the microstructure in both the surface and the bulk. Phosphorus-doped, oxygen-free copper has been cathodically charged with hydrogen for up to 3 weeks. The amount of hydrogen as a function of the distance from the surface was measured by two methods: glow discharge optical emission spectrometry and melt extraction. The penetration of the increased hydrogen content was about 50 μm. Extensive bubble formation took place during the charging. A model has been formulated for the diffusion of hydrogen into the copper, the bubble formation and growth. The model can describe the total amount of hydrogen, the number of bubbles and their sizes as a function of the distance from the surface. Bubbles close to the surface caused the surface to bulge due to the high hydrogen pressure. From the shape of the deformed surface, the maximum hydrogen pressure could be estimated with the help of stress analysis. The maximum pressure was found to be about 400 MPa, which is almost an order of magnitude larger than previously recorded values for electroless deposited copper.

Å. Martinsson (✉) · R. Sandström
Swerea KIMAB, Box 7047, 164 07 Kista, Sweden
e-mail: asa.martinsson@swerea.se

R. Sandström
Department of Materials Science and Engineering, Royal Institute of Technology (KTH), Valhallavägen 79, 114 27 Stockholm, Sweden

Introduction

In Sweden, spent nuclear fuel is planned to be disposed off by encapsulation in waste packages consisting of a cast iron insert surrounded by a copper canister. During storage in the repository, it cannot be ruled out that hydrogen absorption can occur in the copper canister due to corrosion of iron in the presence of water, which might affect the mechanical properties and integrity of the copper canister.

Absorption of hydrogen in copper and the influence of hydrogen on the mechanical properties and the role of the microstructure have been studied for over 50 years. Several studies have focused on charging methods for copper and optimisation of electrochemical charging parameters. Nakahara and Okinaka [1] listed three different charging methods: thermal charging, electrochemical charging and hydrogen entrapment during electroless copper deposition, and described the advantages and drawbacks. Panagopoulos and Zacharopoulos [2] and Al-Marahleh and El-Amoush [3] studied the influence of current density and charging time on the mechanical properties of pure copper. In a later publication, Nakahara and Okinaka [4] discussed how addition of arsenic to the electrolyte used in electrochemical charging ameliorates the absorption of hydrogen, which has now become the standard procedure.

Hydrogen absorption has been proven to have a significant effect on the mechanical properties in thin foils or sheets of copper and copper alloys. Kim and Byrne [5] showed that the hardness is raised by hydrogen charging. Nieh and Nix [6] found that an increased hydrogen and oxygen content in foils shortens the creep life by 10–100 times and reduces the creep strain by a factor 2–3. Nakahara [7] and Okinaka and Straschil [8] showed that trapped hydrogen in copper deposits reduces the ductility.

The absorption and the diffusion of hydrogen in copper are affected by the microstructure. Wampler et al. [9] suggest that impurities (unspecified) can act as hydrogen trapping sites, increasing the hydrogen content in the material. It has also been shown that hydrogen charging of pure copper can nucleate and grow bubbles of hydrogen or, in the presence of oxygen, of water [4, 6, 7, 9–11]. The literature review of Condon and Schober [11] describes various mechanisms causing bubbles to grow, which eventually can create microcracks.

Studies on the subject of hydrogen charging known to the authors are based on hydrogen-charged foils or thin sheets. No studies include the hydrogen depth profile of copper samples thicker than ~2 mm. The thickness of the copper canister intended for nuclear fuel waste is 50 mm. Hence, it is necessary to understand how the introduced hydrogen affects the bulk. In the present paper, the hydrogen depth profile after cathodic charging of oxygen-free, phosphorus-doped copper (Cu-OFP) was determined. Compared to the long storage time in the repository, the alleged corrosion process would be significantly more rapid. The hydrogen charging is accelerated to give manageable charging times. Statistical data of the distribution of hydrogen bubbles created during charging was collected in a metallographic examination. A model for growth of hydrogen bubbles was developed.

Experimental

Tested material is as-forged Cu-OFP provided by the Swedish nuclear fuel and waste management company (SKB). The material is taken from a canister lid with the designation TX104. The chemical composition is found in Table 1. Hydrogen charging was performed on three forms of copper as-received, annealed and 20 % cold-worked bars and plates. The plates, which were analysed with glow discharge optical emission spectrometry (GDOES), had a size 40 × 40 × 10 mm and the bars, which were analysed with melt extraction, had a diameter of 5 or 7 mm. The annealing was performed in a 600 °C salt bath for 5 min, followed by a rapid quench in water. The cold-work in the plates was obtained by reducing the height 15 % by cold rolling, which corresponds to 20 % uniaxial deformation. The bars were strained to 20 % elongation in a tensile testing machine to obtain the same amount of cold-work as the plates. All specimens were electropolished in 50 % orthophosphoric acid for a few minutes to remove oxides and the surfaces were cleaned before cathodic hydrogen charging.

Table 1 Chemical analysis in wt. ppm of the tested material

Ag	As	Fe	Ni	O	P	S	Sb	Cu + P
13	<1	2	2	1–2	45–60	5	1	≥99.99 %

Cathodic charging was used for the introduction of hydrogen. A general description of the method is given in [1]. A constant current was applied over the specimen and a platinum counter electrode. All specimens were charged in 10 % H_2SO_4 electrolyte. An amount of 30 mg/l As_2O_3 was added to the electrolyte as a hydrogen recombination inhibitor. The specimens were charged for 8 or 504 h (3 weeks) at 10 mA/cm^2. All bars and plates were charged separately.

The hydrogen content and depth profile were measured by two different analysis methods. The hydrogen profile in the plates was characterised with GDOES by means of a depth profiling analysis. The advantage of this method is that the depth profile is continuous. A drawback is that the method is not fully quantitative for hydrogen due to the relatively high background equivalent concentration (BEC) of hydrogen in copper, but the method permits comparison between different samples [12].

The bars were analysed by melt extraction using a Leco Rhen602 hydrogen determinator. After charging, each bar was divided into 2 or 3 sections: one section was used as reference and for the others a layer of varying thickness was removed from the surface by turning, see Fig. 1. Each section was divided into two equally long parts before hydrogen analysis. The hydrogen contents in the removed layers were then calculated by comparing the hydrogen content in the analysed bulk samples within the same bar. All specimens were analysed immediately after the charging was completed or stored in liquid nitrogen until the analysis was performed. The two-step profile measurements, consisting of one reference section and one section that was turned, were performed on Ø 5-mm bars. The three-step profile measurements, consisting of one reference section and two sections turned to different thicknesses, were performed on Ø 7-mm bars. Four to six bars were tested at each set of parameters of charging and layer thickness to obtain statistically significant results. This is a coarse method concerning depth variation, but it gives quantitative values of the hydrogen content in the analysed material.

A microscopic examination of the as-received, hydrogen-charged plates was performed using a JEOL 7001

Fig. 1 Schematic drawing of a three-step profile bar after hydrogen charging and turning. After hydrogen charging, the *bar* is turned in sections. The left section is left intact while on the two sections to the right a thin layer is removed by turning. Each section is then divided into two pieces before the hydrogen content is determined

FEG-SEM equipped with INCA Feature. The software INCA Feature provides methods of automated detection and classifications of particles or voids by means of morphology, chemistry and position, which makes it possible to collect statistical data from a large area. A cross section of the specimens was ground and polished with diamond paste before collecting statistical data of the bubbles with Inca Feature. The same specimens were then etched before the SEM images were captured.

Results

Hydrogen depth profile

The hydrogen content of the copper before hydrogen charging was measured by melt extraction in at least four samples for each material condition, see Table 2. The first hydrogen depth profile in as-received and annealed bars was measured after 8-h electrochemical charging. For these specimens, one layer was removed from the surface of each bar, giving a hydrogen depth profile in two steps. One of the annealed bars was turned in three steps. The results are shown in Fig. 2a, b, where the horizontal length of the lines correspond to the width and the position of the layers, and the vertical position indicate the average hydrogen content in each layer. Despite the varying thickness of the layers, the average content in the bar after turning is approximately the same, which would imply that the penetration depth of the hydrogen after 8 h is smaller than 100 μm.

The hydrogen depth profiles of as-received, annealed and 20 % cold-worked Cu-OFP bars were also measured after 3 weeks of hydrogen charging. Two layers of different thickness were removed from each bar, resulting in a three-step hydrogen depth profile. These profiles are presented in Fig. 2c, e together with GDOES curves for Cu-OFP with the same material condition. Thinner layers were removed from the hydrogen-charged bars in the three-step profile compared to those in the two-step profile. Despite the reduced layer thickness, the hydrogen content in both the second and third steps resulted in a value close to the hydrogen content before charging in most bars.

A depth profile after hydrogen charging on two specimens from each material condition was analysed by means of GDOES. Every third analysis was performed on a calibration sample containing no hydrogen, denoted H zero in Fig. 2. The hydrogen depth profile was also measured on two as-received copper specimens before charging, denoted ref 1 and 2.

Table 2 Hydrogen content in the material prior to hydrogen charging

Material condition	Hydrogen content (wt. ppm)
As-received	0.58 ± 0.03
Annealed	0.34 ± 0.10
Cold-worked	0.58 ± 0.07

The GDOES measurements on hydrogen-charged Cu-OFP give a somewhat steeper profile than the values from the machined bars. This gives an indication of the uncertainties in the measured GDOES and machined bar results. The machined bars should in principle give more accurate results, but the scatter in the data is quite significant.

Microstructure

The metallographic examination of hydrogen-charged specimens performed in a FEG-SEM showed that bubbles up to a few μm in size were formed close to the surface of the specimens. Figure 3 shows a typical cross section after charging. Most of the bubble formation has occurred no further away from the surface than ~50 μm. The bubbles were preferably formed at grain boundaries, twins and triple joints, see Fig. 4. Bubbles close to the surface are generally larger than those located further away from the surface and it is not rare that the bubbles are close or even overlapping along the grain boundaries like a string of pearls, see Fig. 5. Smaller bubbles, ≤100 nm, were located both at grain boundaries and within the grains. Larger intragranular bubbles were typically found at very small distances from grain boundaries or twins, Fig. 6. Growth of hydrogen bubbles gives rise to plastic deformation. This is evident by the deformed surface close to bubbles, Fig. 7.

Modelling of hydrogen diffusion taking bubble formation into account

Model

If the diffusion of hydrogen into the material is controlled just by conventional diffusion of hydrogen atoms, it would satisfy the diffusion equation

$$\frac{dc_H}{dt} = D\frac{d^2c_H}{dy^2} \quad (1)$$

where c_H is the hydrogen concentration in solid solution, t is the time, D is the diffusion constant for hydrogen and y is the distance from the surface. Measurements of the diffusion coefficient also close to room temperature are available, see Fig. 8. The values of Ishikawa and McLellan [13] have been used in the present study. With Einstein's expression, the penetration depth y_H can be estimated

$$y_H = \sqrt{2Dt} \quad (2)$$

at room temperature $D = 2.2 \times 10–14$ m/s^2 and with $t = 3$ weeks, we find that the penetration depth is 280 μm,

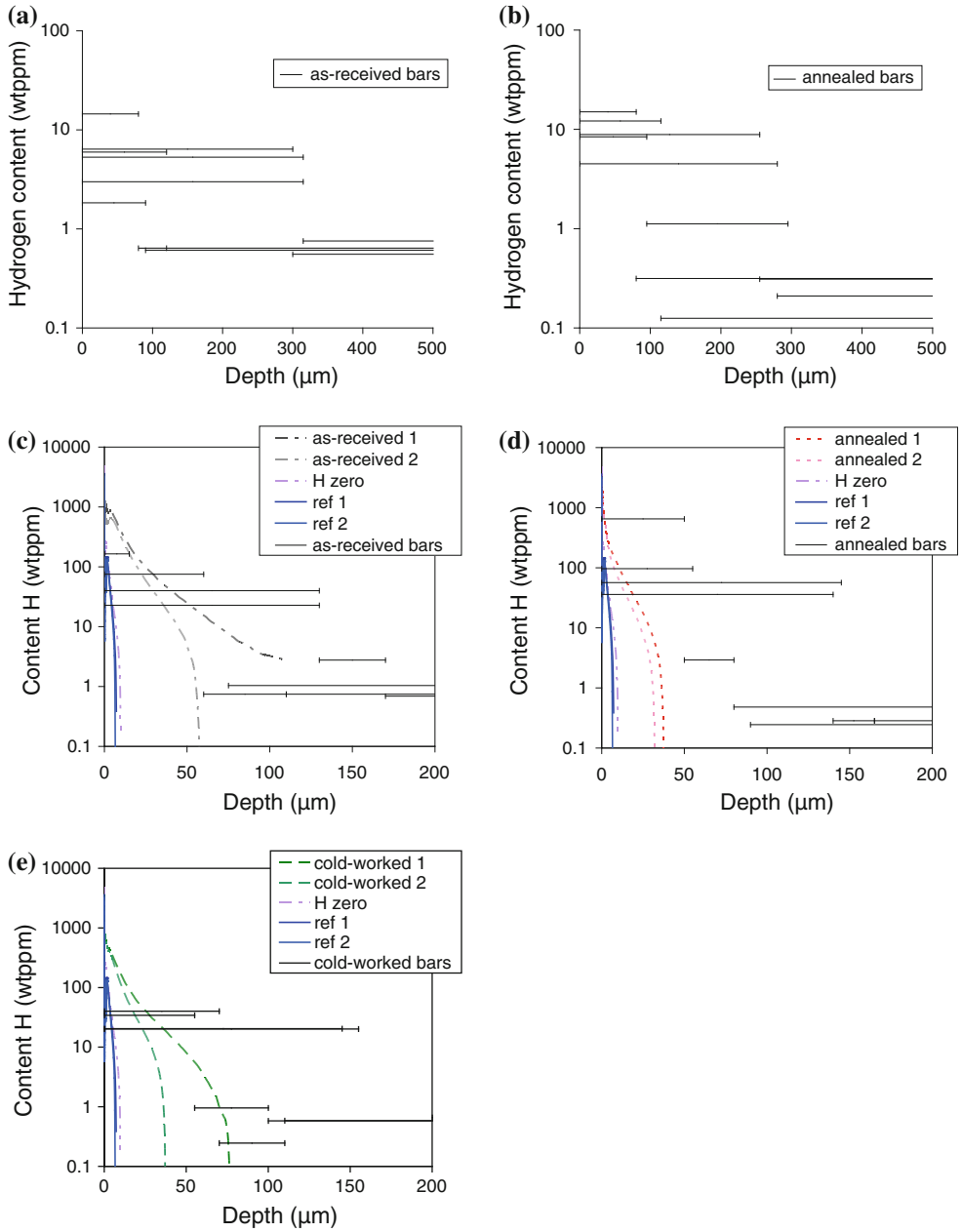

Fig. 2 Hydrogen profile in two steps after 8-h charging of **a** 6 *bars* of as-received Cu-OFP and **b** 5 *bars* of annealed Cu-OFP, and in three steps after 3-weeks charging of **c** 4 *bars* of as-received Cu-OFP, **d** 4 *bars* of annealed Cu-OFP, and **e** 4 *bars* of 20 % cold-worked Cu-OFP together with hydrogen profile from 2 plates in each material condition after 3 weeks of charging measured by GDOES

considerably larger than the observed value of about 50 μm.

The hydrogen flux to bubbles must also be considered. Hydrogen atoms diffuse to bubbles where they form hydrogen molecules. The diffusion from bubbles back to the matrix is neglected due to low concentration of atomic hydrogen in the bubbles. Transfer of hydrogen to bubbles was analysed by Wampler et al. [9]. They proposed the following relation for the hydrogen flux J_{H} to a bubble

$$J_H = D\nabla c_H = D\frac{c_H}{r} \tag{3}$$

where r is the bubble radius. This inflow gives rise to growth of the bubbles.

$$\frac{dr}{dt} = \frac{D}{\rho_{\mathrm{H}}}\frac{c_H}{r} \tag{4}$$

ρH is the density of hydrogen in the bubbles [kg/m^3]. Experimentally, it is known that quite a high hydrogen

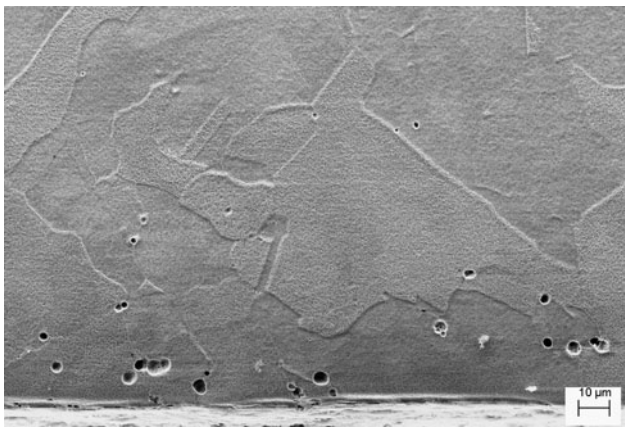

Fig. 3 A typical cross section of one of the as-received hydrogen-charged specimen for 3 weeks. Most bubbles formed during charging are situated within 50 µm from the surface. The surface is the bright *horizontal line* located at the bottom of the image

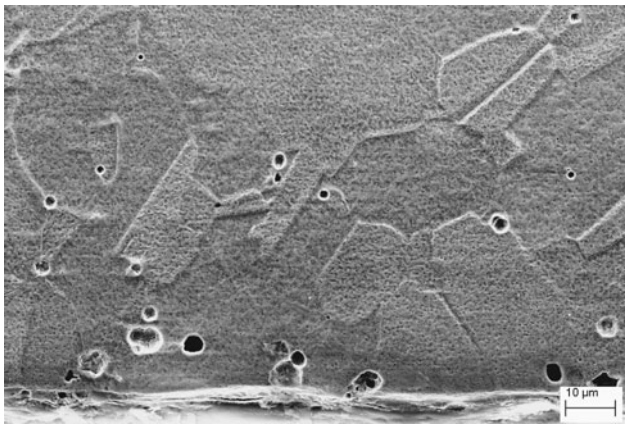

Fig. 4 Another part of the cross section at higher magnification. The bubbles are preferably formed close to the surface, located at the bottom of the image and at grain boundaries

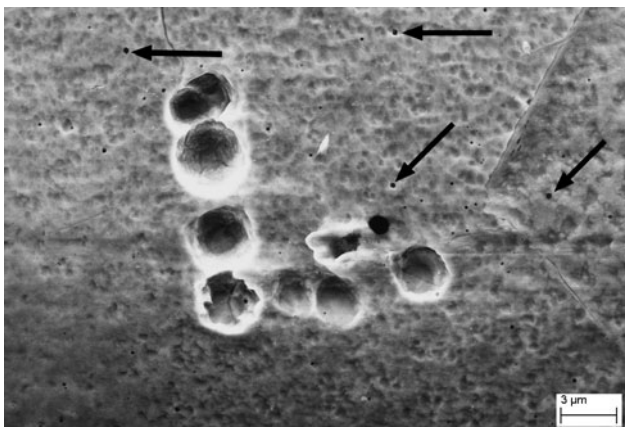

Fig. 5 Larger bubbles at grain boundaries and smaller intragranular bubbles marked with arrows. The surface of the specimen is located horizontally about 10 µm below the bottom border of the image

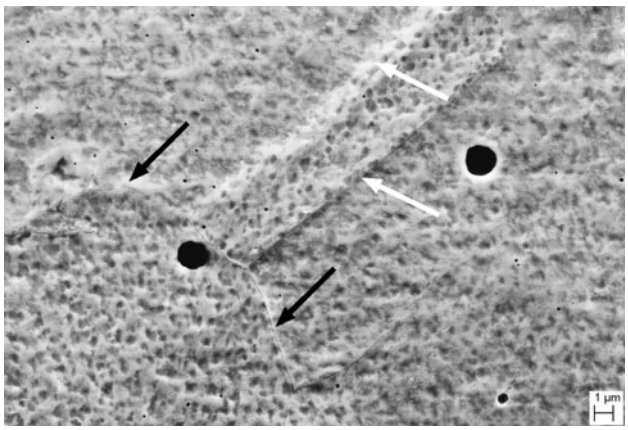

Fig. 6 Two smaller hydrogen bubbles close to grain boundary (*black arrows*) and twins (*white arrows*). The image is located about 40 µm from the surface

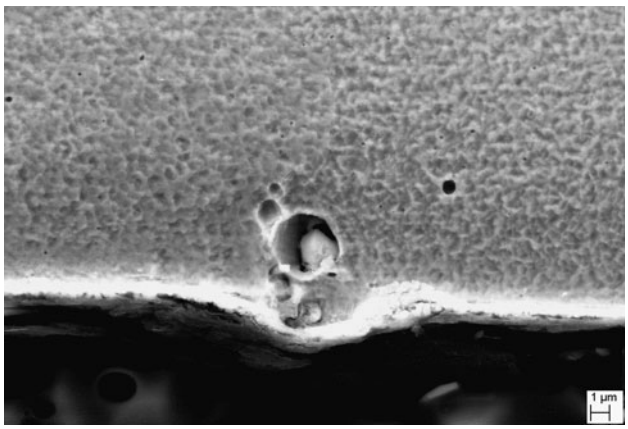

Fig. 7 Surface deformation due to hydrogen bubble close to the surface

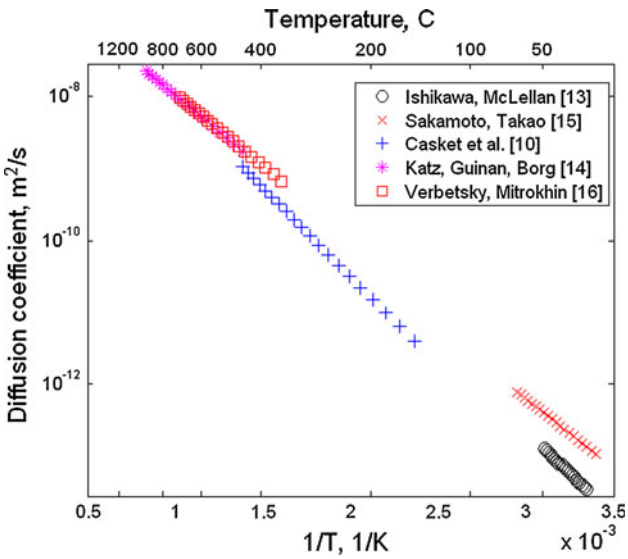

Fig. 8 Diffusion coefficient for hydrogen in copper versus inverse absolute temperature. Experimental data from [10, 13, 19–21]

pressure is needed to make the bubbles grow [11]. The magnitude of the hydrogen pressure will be analysed below.

Concerning the number of bubbles per unit volume n_V, one bubble containing H^2 in each grain boundary corner is assumed. With the help of conventional stereology, n_V can be related to the number of bubbles per unit area n_A.

$$n_A = 2rn_V \tag{5}$$

The change of H^2 concentration c_H due to the flux into the bubbles is, cf. Eq. (3)

$$\frac{dc_H}{dt} = -4\pi r^2 n_{V por} D \frac{c_H}{r} \tag{6}$$

Adding this contribution to (1) and using (5) gives the modified diffusion equation

$$\frac{dc_H}{dt} = D\frac{d^2c_H}{dy^2} - 2\pi n_A D c_H \tag{7}$$

Equations (4) and (7) constitute a system for bubble radii and hydrogen content that can be solved numerically. The first boundary condition concerns the charging rate of hydrogen through the surface that is assumed to be 1×10^{-10} kg/m^2/s. Since this parameter cannot be predicted, it has to be verified by checking that the total computed hydrogen content agrees with the experimental values. For the model values presented below, this is satisfied. Equation (7) is solved over a distance of 200 μm. The second boundary condition is that the derivative of the hydrogen concentration at this depth is zero.

In the past, attempts have been made to estimate the internal pressure of hydrogen bubbles by dislocation loop punching mechanisms. However, pressures in the GPa range have been obtained that are not consistent with observations [11, 14]. Instead the pressure must be found from the geometry of observed bubbles. For this purpose, the shape of bubbles has been analysed. A finite element model (FEM) of a bubble close to the surface has been set up. An axisymmetric bubble geometry is assumed, Fig. 9. After the pressure is applied, the bubble expands. This is marked with the white area in Fig. 9. This geometry simulates several observed bubbles close to the surface. One example is given in Fig. 7. From the geometry of the bubble, it can be seen that it has collapsed, i.e. it has expanded due to internal hydrogen pressure and finally collapsed by leakage. This can be concluded from the FEM analysis since a bubble cannot deform much more than in Fig. 9, before it becomes unstable and grows until it fails.

Accurate stress–strain relations for Cu-OFP are available. The following relation has been used in the stress analysis [15]

$$\sigma = \sigma_y + k(1 - e^{-\Omega\varepsilon}) \tag{8}$$

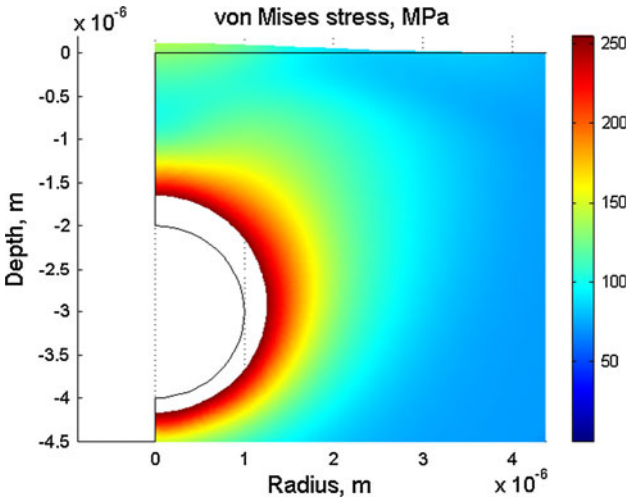

Fig. 9 Stress analysis of a bubble close to collapse due to hydrogen pressure of 400 MPa. Von Mises stress. Axisymmetric geometry

where $\sigma_y = 71$ MPa is the yield strength, ε is the strain and $k = 188$ MPa and $\Omega = 7.33$ are constants. At the pressure 400 MPa, the bubble size has increased due to plastic deformation. In Fig. 9, the original bubble radius is 1 μm. After the pressure has been applied, the bubble expands to a radius of 1.3 μm. The expansion is slightly larger at the upper side due to the proximity of the surface. At the surface above the bubble, a change in shape is also observed. Higher pressures than 400 MPa are not possible to apply without the bubble becoming unstable.

As pointed out above, the bubble in Fig. 7 has collapsed. For another bubble with almost identical geometry and distance from the surface (not shown), the surface outside the bubble has only bulged marginally indicating that it has not collapsed. For this reason, the limit pressure is close to 400 MPa. An upper limit for the hydrogen pressure is the collapse load for the expanded bubble that corresponds to a pressure of 480 MPa. Similar results have been obtained for several bubbles. In the analysis, 400 MPa has been assumed since the maximum hydrogen pressure must be close to the maximum value that is stable in the FEM modelling. An analytical estimate of the maximum pressure can be obtained from the collapse pressure p_{lim} of a thick sphere with inner radius R_i and outer radius R_y

$$p_{lim} = 2(\sigma_y + k)\ln\frac{R_y}{R_i} \tag{9}$$

$\sigma_y + k$ is approximately the true tensile strength. Equation (9) is evaluated for the same geometry as in Fig. 9. The inner radius is taken as the bubble radius $R_i = 1.31$ μm (expanded geometry) and the outer radius as the distance to the surface $R_y = 3$ μm. This gives a limit pressure $p_{lim} = 429$ MPa (expanded bubble) and 569 MPa (original bubble size). Since the real bubble is backed by more

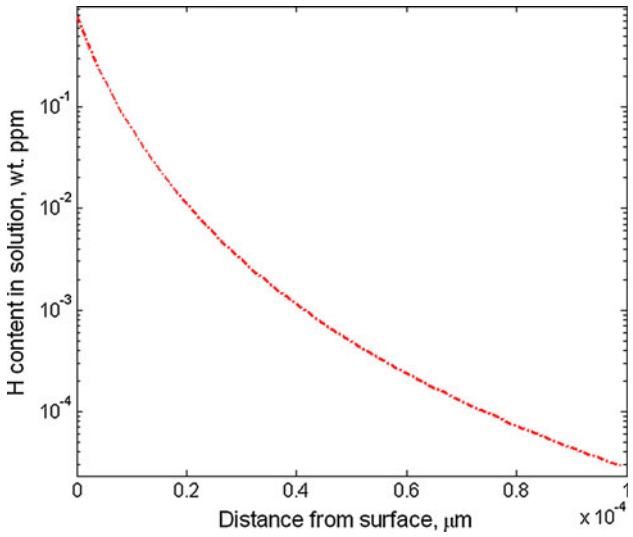

Fig. 10 Hydrogen in solid solution as a function of distance from the surface after 3 weeks of charging

material than a sphere of the specified dimension, the FEM results give a slightly higher pressure limit. Since the dimensions of the critical bubble appear in a logarithmic factor in Eq. (9), the limit pressure is not dramatically dependent on the bubble geometry.

Application of the model

Equation (7) gives the following distribution of hydrogen in solid solution (see Fig. 10). The amount decreases quite rapidly with distance from surface. It is interesting to compare the results with values for solid solution in thermal equilibrium. No experimental values exist at room temperature. However, McLellan [16] measured values in the temperature interval 600–1,050 °C. The Arrhenius expression in Eq. (10) gives quite an accurate fit to these data

$$H_{\mathrm{sol}} = Be^{-\frac{Q}{RT}} \tag{10}$$

where $B = 181$ wt. ppm and $Q = 54850$ J/mol. R and T have their conventional meaning. If Eq. (10) is extrapolated down to room temperature, it gives a solubility of only 4×10^{-8} wt. ppm. This is, however, likely to underestimate the real value since the activation energy Q can be expected to decrease at lower temperatures. Due to the low solubility of hydrogen there is no surprise that there is ample bubble formation.

The model values for the bubble diameters are shown in Fig. 11. The observations for bubbles have been placed in classes according to the distance from the surface. The class width is 2 μm. The values in Fig. 11 are average bubble sizes in each class. The computed bubble diameters are in reasonable agreement with the observations.

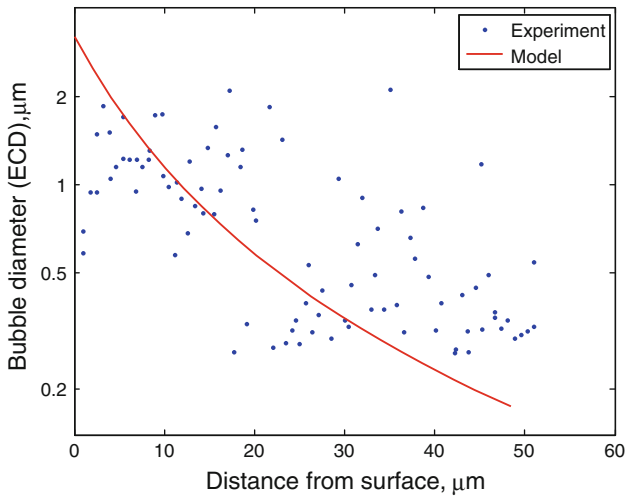

Fig. 11 Bubble diameter (*equivalent circle* diameter, ECD) as a function of distance from the surface after 3 weeks of charging

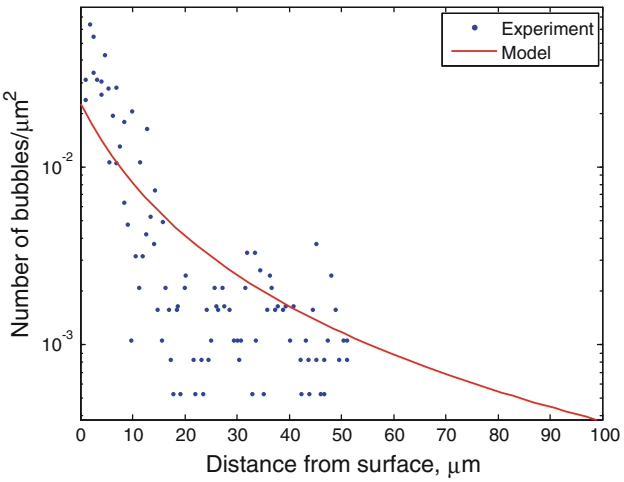

Fig. 12 Number of bubbles per unit area as a function of distance from the surface after 3 weeks of charging

The number of bubbles per unit area is compared to experimental results in Fig. 12. Again, an acceptable comparison is found. The corresponding graph for the bubble area fraction is shown in Fig. 13. A favourable agreement is obtained. In Fig. 14, the total hydrogen content is given as a function of distance from the surface. Model values are obtained by multiplying the bubble area fraction with the hydrogen density in the bubbles. In the same way, the metallographic values are the measured area fraction in each size class multiplied by the hydrogen density. GDOES data are shown for as-received and annealed material. The main difference between the model and experiments is the high model values close to the surface. Some bubbles might vanish at the surface due to outflow of hydrogen, which is not taken into account in the

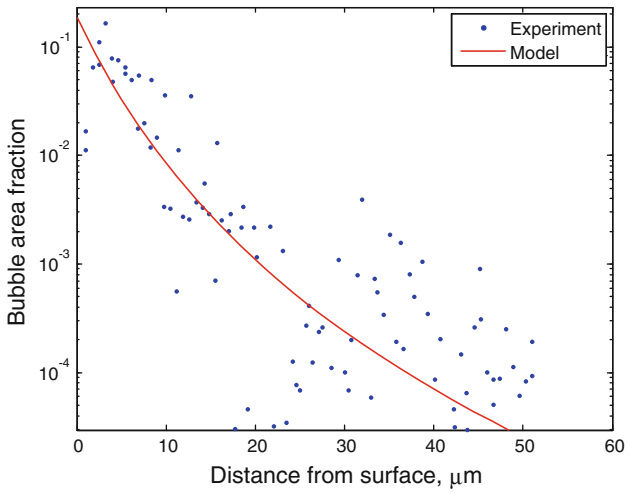

Fig. 13 Bubble area fraction as a function of distance from the surface after 3 weeks of charging

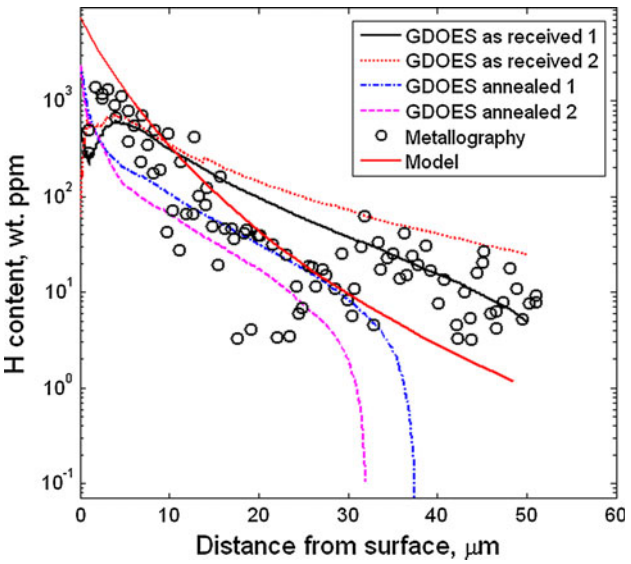

Fig. 14 Total hydrogen content versus distance from the surface after 3 weeks of charging. Model values are compared to the metallographic observations and GDOES measurements

model. It is interesting to note that the metallographic and the GDOES measurements are in close agreement.

Discussion

The objective of this study was to understand how hydrogen absorption in Cu-OFP bulk material influences the microstructure and how the absorbed hydrogen is distributed in the material. The results from the two-step hydrogen profile showed that the penetration depth of the absorbed hydrogen was <100 μm. The three-step profile was improved by reducing the layer thicknesses to a minimum allowed by the turning equipment, and prolongation of the charging time from 8 h to 3 weeks to reduce the variation between the bars. Some variations between bars still exist, but in general it can be concluded from the melt extraction analysis that the hydrogen absorption is higher in as-received and annealed copper than in the cold-worked copper. This was not expected since hydrogen transport along dislocations was anticipated. During 3 weeks of charging, the average hydrogen content in the topmost 50 μm increased from 0.6 to almost 100 wt. ppm in as-received copper. The hydrogen content in the bulk is constant. The annealing before charging reduces the hydrogen content to half the original value, but the annealing does not seem to affect the final hydrogen content after charging. The hydrogen content in the outer 50 μm in cold-worked material after hydrogen charging is only about 40 wt. ppm, which is considerably lower.

The GDOES analyses show that hydrogen penetration depth is only a few tens of micrometres. The hydrogen content is the highest at the surface and diminishes exponentially with distance from surface. In contrast to the results from the three-step profile, the GDOES results show that the hydrogen absorption is the highest in the as-received copper and the absorption in the cold-worked copper is slightly higher than in the annealed copper. Taking the accuracy of the measurements of both depth profile methods into consideration, the GDOES depth profiles fit the results from the 3-step method rather well, but additional analyses are required to determine the influence of the pre-charging material condition on the hydrogen absorption.

The measured hydrogen content in the charged copper highly exceeds the solubility limit of hydrogen in copper at room temperature [16]. Hence, only a small fraction of the absorbed hydrogen is in solid solution. The remaining hydrogen must be trapped in the material in another form. Owing to the absence of oxygen, it is probable that the hydrogen accumulates in the form of H_2 gas in the bubbles observed in the microscopic examination [9]. The absence of bubbles in the as-received copper before charging confirmed that the bubbles are due to the increased hydrogen content. The distribution of the bubbles is consistent with the penetration depth determined by both the analysis methods. Recombination of hydrogen atoms in the surface layer of the specimen would significantly affect the measured diffusion rate of hydrogen atoms in the material [11]. The accumulation of hydrogen molecules in bubbles would thus explain why the bulk content of hydrogen remained constant. One could argue that the high hydrogen content in the bubbles turns out to be a diffusion obstacle, preventing the hydrogen atoms to diffuse further into the material. Of all examined bubbles, only one was found to contain a particle, see Fig. 7. Furthermore, no impurities

have been found in or between grains. Hence, our conclusion is that there are no impurities or inclusions acting as hydrogen entrapment sites.

Several bubbles were observed close to the surface, where plastic deformation has taken place and the bubbles must be near collapse. Some of these bubbles have been simulated with FEM applying different pressures. The bubbles were found to be stable up to a pressure of about 400 MPa. The collapse pressure assessed with FEM gave a value of around of 480 MPa. From these results, it was concluded that hydrogen pressures up to 400 MPa are present in the charged copper. This is an order of magnitude higher than in previous investigations for electroless deposited copper. Nakahara and Okinaka [17] found a pressure of 25–40 MPa, and Graebner and Okinaka [18] about 68 MPa. The maximum pressure is lower in these cases is because specimens were in the form of thin films and that electroless-deposited copper is a non-dense material in general.

A model has been formulated for diffusion of hydrogen into the copper. In the model, it is assumed that hydrogen atoms diffuse into the copper. Most of the hydrogen atoms end up in bubbles where they combine to hydrogen molecules. The hydrogen in the bubbles reaches a high pressure that gives rise to plastic deformation and expansion of the bubbles. This explains the observed bubble formation and growth. In the model, the diffusion of hydrogen from the bubbles to the matrix is neglected. There are two reasons for this. First, the concentration of dissociated hydrogen atoms is low. Second, the estimated amount of hydrogen in solid solution is quite low, far below 1 wt. ppm. However, the amount is still much higher than the equilibrium value in solid solution that is obtained by extrapolation from high temperature measurements. The model can describe the observed bubble diameter, the number of bubbles and the bubble area fraction as a function of distance from the surface. These quantities decrease approximately exponentially with increasing distance from the surface. This is natural since both, the total amount of hydrogen and the amount in solid solution, decrease exponentially from the surface. The variation of the total hydrogen content as a function of distance from the surface is consistent both with the GDOES measurements and the metallographic observations assuming the measured maximum hydrogen pressure in the bubbles.

Conclusions

It has been shown that electrochemical charging of Cu-OFP bulk samples strongly increases the hydrogen content in the surface layer. The penetration depth is about 50 μm and the hydrogen content in the bulk is unaffected. Annealing of the copper reduces the initial hydrogen content, but does not seem to affect the absorption of hydrogen during charging much. Supersaturation of hydrogen in Cu-OFP results in the formation and growth of hydrogen gas bubbles mainly at grain boundaries.

From the shape of bubbles that have bulged close to the surface, the maximum hydrogen pressure in the bubbles has been found to be about 400 MPa by means of elasto-plastic stress analysis. With a simple expression for the limit pressure of a thick-walled sphere, the maximum pressure can also be estimated.

A model has been formulated for hydrogen diffusion taking bubble formation into account. The model can describe the distribution of the bubble sizes and their numbers, their radii and hydrogen content.

Acknowledgements The authors would like to thank the Swedish Nuclear Fuel and Waste Management Co (SKB) for providing financial support of this study. The authors would also like to express their gratitude to Mr J. Ahlström, Swerea KIMAB, for his work with the hydrogen charging, Mr Martin Lundholm and Mr Mats Randelius, Swerea KIMAB, for their help with hydrogen analyses and Dr. Henrik Andersson-Östling, Dr. Rui Wu, Swerea KIMAB and Christina Lilja, SKB, for fruitful discussions and critical comments on the manuscript.

References

1. Nakahara S, Okinaka Y (1988) Mater Sci Eng A 101:227
2. Panagopoulos CN, Zacharopoulos N (1994) J Mater Sci 29(14):3843. doi:10.1007/BF00357357
3. Al-Marahleh GS, El-Amoush AS (2005) Am J Appl Sci 2(2):526
4. Nakahara S, Okinaka Y (1989) J Electrochem Soc 136(7):1892
5. Kim JJ, Byrne JG (1985) Mater Sci Eng 74(2):201
6. Nieh TG, Nix WD (1980) Acta Metall 28(5):557
7. Nakahara S (1988) Acta Metall 36(7):1669
8. Okinaka Y, Straschil HK (1986) J Electrochem Soc 133(12):2608
9. Wampler WR, Schober T, Lengeler B (1976) Philos Mag 34(1):129
10. Caskey JGR, Dexter AH, Holzworth ML, Louthan JMR, Derrick RG (1975) Hydrogen transport in copper. Paper presented at the Materials Science Symposium of AIME, Cincinnati, Nov 11–13
11. Condon JB, Schober T (1993) J Nucl Mater 207((C)):1
12. Angeli J, Bengtson A, Bogaerts A, Hoffmann V, Hodoroaba VD, Steers E (2003) Glow discharge optical emission spectrometry: moving towards reliable thin film analysis—a short review. J Anal At Spectrom 18(6):670
13. Ishikawa T, McLellan RB (1985) J Phys Chem Solids 46(4):445
14. Kamada K, Sagara A, Kinoshita H, Takahashi H (1988) Scr Metall 22(8):1281
15. Sandström R, Hallgren J (2012) J Nucl Mater 422:51
16. McLellan RB (1973) J Phys Chem Solids 34(6):1137
17. Nakahara S, Okinaka Y (1983) Acta Metall 31(5):713
18. Graebner JE, Okinaka Y (1986) J Appl Phys 60(1):36
19. Katz L, Guinan M, Borg RJ (1971) Phys Rev B 4(2):330
20. Sakamoto Y, Takao K (1982) Nippon Kinzoku Gakkai-si 46(3):285
21. Verbetsky VN, Mitrokhin SV (2000) Diffus Defect Data PtB 73:503